

Statistics of shear-induced rearrangements in a two-dimensional model foam

Shubha Tewari,^{1,2} Dylan Schiemann,² Douglas J. Durian,¹ Charles M. Knobler,² Stephen A. Langer,³ and Andrea J. Liu²

¹*Department of Physics and Astronomy, University of California, Los Angeles, Los Angeles, California 90095*

²*Department of Chemistry and Biochemistry, University of California, Los Angeles, Los Angeles, California 90095*

³*Information Technology Laboratory, NIST, Gaithersburg, Maryland 20899*

(Received 1 April 1999)

Under steady shear, a foam relaxes stress through intermittent rearrangements of bubbles accompanied by sudden drops in the stored elastic energy. We use a simple model of foam that incorporates both elasticity and dissipation to study the statistics of bubble rearrangements in terms of energy drops, the number of nearest neighbor changes, and the rate of neighbor-switching ($T1$) events. We do this for a two-dimensional system as a function of system size, shear rate, dissipation mechanism, and gas area fraction. We find that for dry foams, there is a well-defined quasistatic limit at low shear rates where localized rearrangements occur at a constant rate per unit strain, independent of both system size and dissipation mechanism. These results are in good qualitative agreement with experiments on two-dimensional and three-dimensional foams. In contrast, we find for progressively wetter foams that the event size distribution broadens into a power law that is cut off only by system size. This is consistent with criticality at the melting transition. [S1063-651X(99)06610-6]

PACS number(s): 83.70.Hq, 83.50.Ax, 82.70.Kj, 82.70.Rr

I. INTRODUCTION

A foam is a disordered collection of densely-packed poly-disperse gas bubbles in a relatively small volume of liquid [1–3]. Foams have a rich rheological behavior; they act like elastic solids for small deformations but they flow like viscous liquids at large applied shear stress [4]. The stress is relaxed by discrete rearrangement events that occur intermittently as the foam is sheared. Three-dimensional foams are opaque, which makes it difficult to observe these bubble movements directly. However, measurements [5,6] by diffusing-wave spectroscopy of three-dimensional foams subjected to a constant shear rate suggest that the number of bubbles involved in the rearrangements is small, of the order of four bubbles. Bubble rearrangements can be observed directly by fluorescence microscopy in two-dimensional foams found in insoluble monolayers at the air-water interface. A study of shear in such foams [7] also revealed no large-scale rearrangements.

While analytical theories for the response to applied steady shear may be constructed for periodic foams [4], only simulation approaches are possible for disordered foams. Kawasaki's [8] vertex model was the first to incorporate dissipative dynamics. It applies to a two-dimensional foam in the limit in which the area fraction of gas is unity (a dry foam). Bubble edges are approximated by straight line segments that meet at a vertex that represents a Plateau border. The equations of motion for the vertices are solved by balancing viscous dissipation due to shear flow within the borders by surface tension forces. At low shear rates, the elastic energy of the foam, which is associated with the total length of the bubble segments, shows intermittent energy drops with a distribution of event rate vs. energy release that follows a broad power law, consistent with self-organized criticality. The rearrangements associated with the largest events consist of cooperative motions of bubbles that extend over much of the system.

Weaire and co-workers [9–11] were the first to develop a

model appropriate to a disordered wet foam. The model does not include dissipation. The effect of shear is studied in the quasistatic limit; that is, the system is allowed to relax to an equilibrium configuration after each of a series of infinitesimal shear steps. The size of rearrangements is measured by the number of changes in nearest-neighbor contacts. For dry foams, the average event size is small, inconsistent with a picture of self-organized criticality. However, as the liquid content increases, the event-size distribution broadens, with the largest events involving many bubbles. Although the statistics are limited, this is consistent with a picture of criticality at the point where the foam loses its rigidity.

The first model capable of treating wet, disordered foams at nonzero shear rate was proposed by Durian [12]. His model pictures the foam as consisting of spherical bubbles that can overlap. Two pairwise-additive interactions between neighboring bubbles are considered, a harmonic repulsive force that mimics the effect of bubble deformation and a force proportional to the velocity difference between neighboring bubbles that accounts for the viscous drag. He found [13] that the probability density of energy drops followed a power law, with a cutoff at very high energy events. The largest event observed consisted of only a few bubbles changing neighbors. This is inconsistent with a picture of self-organized criticality, although the effect of the liquid content on the topology statistics was not examined.

Most recently, Jiang *et al.* [14] have employed a large- Q Potts model to examine sheared foams. In this lattice model bubbles are represented by domains of like spin, and the film boundaries are the links between regions of different spins. Each spin merely acts as a label for a particular bubble, and the surface energy arises only at the boundaries where the spins differ. The evolution of the foam is studied by Monte Carlo dynamics with a Hamiltonian consisting of three terms: the coupling energy between neighboring spins at the boundaries of the bubbles; an energy penalty for changes in the areas of the bubbles, which inhibits coarsening of the foam; and a shear term that biases the probability of a spin

reassignment in the strain direction. The spatial distribution of $T1$ events was examined and no system-wide rearrangements were observed. Nevertheless, Jiang *et al.* found a power-law distribution of energy changes. They also found that the number of events per unit strain displayed a strong shear-rate dependence, suggesting that a quasi-static limit does not exist.

These four simulation approaches thus offer conflicting pictures as to (1) the existence of a quasistatic limit, (2) whether or not rearrangement dynamics at low shear rates are a form of self-organized criticality, and (3) whether or not the melting of foams with increasing liquid content is a more usual form of criticality. One possible reason for this disagreement is differences in the treatment of dissipation, and hence in the treatment of the *dynamics* of the rearrangements. In principle, the only accurate way in which to include dissipation in a sheared foam is to solve for the Stokes flow in the liquid films and Plateau borders. This approach has been adopted by Li, Zhou, and Pozrikidis [15], but so far it has only been applied to periodic foams. The statistics of rearrangement events are fundamentally different in periodic and disordered foams; in sheared periodic foams, all the bubbles rearrange simultaneously at periodic intervals, while in a disordered foam, the rearrangements can be localized and intermittent. Nonetheless, the Stokes-flow approach is the only one that can be used as a benchmark for more simplified models.

In order to gain a better understanding of the origin of the discrepancies between the various models, as well as between the models and experiments, we report here a systematic study of the properties of a sheared foam using Durian's model. We begin by reviewing his model and discussing our numerical implementation using two different forms of dissipation. After confirming that there are no significant system-size effects for dry samples, we examine the shear-rate dependence and establish the existence of a true quasi-static limit for the distribution and rate of energy drops and topology changes. This limit is shown to be independent of the dissipation mechanism for foams of different gas fractions. Finally, we examine dramatic changes in the behavior of these quantities as the liquid content is tuned toward the melting point.

II. BUBBLE MODEL

Durian's model [12,13] is based on the wet-foam limit, where the bubbles are spherical and just touch. The foam is described entirely in terms of the bubble radii $\{R_i\}$ and the time-dependent positions of the bubble centers $\{\vec{r}_i\}$. The details of the microscopic interactions at the level of soap films and vertices are subsumed into two pairwise additive interactions between bubbles, which arise when the distance between bubble centers is less than the sum of their radii. The first, a repulsion that originates in the energy cost to distort bubbles, is modeled by the compression of two springs in series with individual spring constants that scale with the Laplace pressures σ/R_i , where σ is the liquid-gas surface tension and R_i is the bubble radius. Bubbles that do not overlap are assumed not to interact. The repulsive force on bubble i due to bubble j is then

$$\vec{F}_{ij}^r = k_{ij}[(R_i + R_j) - |\vec{r}_i - \vec{r}_j|]\hat{r}_{ij}, \quad (1)$$

where \hat{r}_{ij} is the unit vector pointing from the center of bubble j to the center of bubble i , and $k_{ij} = F_0/(R_i + R_j)$ is the effective spring constant, with $F_0 \approx \sigma\langle R \rangle$. The second interaction is the viscous dissipation due to the flow of liquid in the films. It, too, is assumed to be pairwise additive and is modeled by the simplest form of drag, where the force is proportional to the velocity difference between overlapping bubbles. The viscous force on bubble i due to its neighbor j is

$$\vec{F}_{ij}^v = -b(\vec{v}_i - \vec{v}_j), \quad (2)$$

where the constant b is proportional to the viscosity of the liquid, and is assumed to be the same for all bubble neighbors.

The net force on each bubble sums to zero, since inertial effects are negligible in this system. Summing over those bubbles j that touch bubble i , the equation of motion for bubble i is

$$\sum_j (\vec{v}_i - \vec{v}_j) = \frac{F_0}{b} \sum_j \left[\frac{1}{|\vec{r}_i - \vec{r}_j|} - \frac{1}{R_i + R_j} \right] (\vec{r}_i - \vec{r}_j) + \frac{\vec{F}_i^a}{b}, \quad (3)$$

where \vec{F}_i^a is an externally applied force, arising, for instance, from interactions with moving walls.

Durian [12,13] employed a further simplification of this model, in which the viscous dissipation is taken into account in a mean-field manner by taking the velocity of each bubble relative to an average linear shear profile. In this case, the total drag force on bubble i due to all of its N_i overlapping neighbors is

$$\vec{F}_i^v = -bN_i(\vec{v}_i - \dot{\gamma}y_i\hat{x}). \quad (4)$$

In the numerical simulations reported here we use both the mean-field model of dissipation as well as the approximation represented by Eq. (2), which we call the local dissipation model. In the latter, at each integration time step the velocity of a bubble is measured with respect to the average of the velocities of its N_i overlapping neighbors, so that the total drag force on bubble i is

$$\vec{F}_i^v = -bN_i \left(\vec{v}_i - \frac{1}{N_i} \sum_{j=1}^{N_i} \vec{v}_j \right). \quad (5)$$

For very large N_i , this reduces to Eq. (4); otherwise, it allows for fluctuations. One aim of our study is to establish the sensitivity of the results to the specific form of dissipation used, Eqs. (4) or (5).

In two dimensions, the area fraction of gas bubbles, ϕ , can be defined by the total bubble area $\Sigma \pi R_i^2$ per system area. Because the bubbles are constrained to remain circular and their interactions are approximated as pairwise-additive [16], the model necessarily breaks down for very dry foams. In fact, bubble radii can even be chosen so that ϕ exceeds one. In a real foam, of course, this is prevented by the divergence of the osmotic pressure.

III. NUMERICAL METHOD

All the results reported here are based on simulations of a two-dimensional version of Durian's model. We use Eq. (3) to study a two-dimensional foam periodic in the x direction and trapped between parallel plates in the y direction. Bubbles that touch the top and bottom plates are fixed to them, and the top plate is moved at a constant velocity in the x direction. (The system can also be sheared with a constant force instead of a constant velocity, but that case will not be discussed here.) Thus bubbles are divided into two categories — “boundary” bubbles, which have velocities that are determined by the motion of the plates, and “interior” bubbles, whose velocities must be determined from the equations of motion.

The equation of motion Eq. (3) can be written in the form

$$\mathbf{M}(\{\mathbf{r}\}) \cdot \{\mathbf{v}\} = \{\mathbf{F}^r\}/b + \{\mathbf{F}^a\}/b, \quad (6)$$

where $\{\mathbf{v}\}$ is a vector containing all the velocity components of all of the bubbles, $\{\mathbf{v}_0^x, \mathbf{v}_0^y, \mathbf{v}_1^x, \mathbf{v}_1^y, \dots\}$, $\{\mathbf{F}^r\}$ is a vector of all of the repulsive bubble-bubble forces, and $\{\mathbf{F}^a\}$ contains all the forces exerted by the walls. The matrix \mathbf{M} depends on the instantaneous positions of the bubbles. The 2×2 block submatrix M_{ij} is a unit matrix $\mathbf{1}$ if the distinct bubbles i and j overlap, and $\mathbf{0}$ if they do not overlap. On the diagonal, $M_{ii} = -\mathbf{1}N_i$, where N_i is the number of overlapping neighbors of bubble i . Equation (6) is of the form $\mathbf{A}(\mathbf{r}, t) \cdot (d\mathbf{r}/dt) = f(\mathbf{r}, t)$, which we solve for the bubble positions \mathbf{r} with the routine DDRIV3 [17]. DDRIV3 has the ability to solve differential equations in which the left hand side is multiplied by an arbitrary time-dependent matrix. Furthermore, it allows all matrix algebra to be performed by external routines, allowing us to take advantage of the sparse nature of \mathbf{M} . We use the SPARSKIT2 [17] library for sparse matrix solutions, and the Runge-Kutta algorithm with a variable time step determined by the error tolerance to integrate the differential equations.

The only relevant dynamical scale in this problem is set by the characteristic relaxation time arising from the competing mechanisms for elastic storage and viscous dissipation, $\tau_d = b\langle R \rangle / F_0$. This is the characteristic time scale for the duration of bubble rearrangements driven by a drop in total elastic energy. Without loss of generality we set this to unity in the simulation. In these units, the dimensionless shear rate $\dot{\gamma}$ is the capillary number.

To introduce polydispersity, the bubble radii are drawn at random from a flat distribution of variable width; in all the results reported here, the bubble radii vary from 0.2 to 1.8 times the average bubble radius. We note that the size distribution in experimental systems is closer to a truncated Gaussian with the maximum size equal to twice the average radius. The truncated Gaussian distribution arises naturally from the coarsening process [18,19]. We tested the sensitivity of our results to the bubble distribution by doing one run with bubbles drawn from a triangular distribution, and found that the shape of the distribution had no significant effect. Similarly, variation of the width of a triangular distribution has been shown to have no influence on the linear viscoelasticity [13]. Note that it is important to include polydispersity because a monodisperse system will crystallize under shear, especially in two dimensions.

In all of our runs, the system is first equilibrated with all bubbles treated as interior bubbles, and with a repulsive interaction between the bubbles and the top and bottom plates so that bubbles cannot penetrate the plates. The bubbles that touch the top and bottom plates are then converted to boundary bubbles. The top plate is moved at a constant velocity and data collection begins after any initial transients die away. The total strain covered by a given run ranges from 10 to 100. In addition to recording quantitative measures of the system, we also run movies of the sheared foam in order to observe visually how the flow changes as a function of shear rate, area fraction and other parameters [20].

IV. QUANTITIES MEASURED

Before showing results, we discuss the various quantities extracted during a run. Under a small applied shear strain, bubbles in a real foam distort; as the shear strain increases, the structure can become unstable and they may thus rearrange their relative positions. In the bubble model, the distortion of bubbles is measured globally by the total elastic energy stored in all the springs connecting overlapping bubbles:

$$E = \sum \frac{1}{2} k_{ij} [(R_i + R_j) - |\vec{r}_i - \vec{r}_j|]^2. \quad (7)$$

Under steady shear, the elastic energy rises as bubbles distort (overlap) and then drops as bubbles rearrange. Thus, the total elastic energy fluctuates around some average value. The scale of the energy is set by the elastic interaction and is of order $F_0 \langle R \rangle$ per bubble, where $\langle R \rangle$ is the average bubble radius.

Figure 1(a) shows a plot of the total elastic energy as a function of strain for a system of 144 bubbles at area fraction $\phi = 1.0$ driven at a constant shear rate of $\dot{\gamma} = 10^{-3}$. Similar plots for stress vs strain are shown in Refs. [12,13]. Note the precipitous energy drops, ΔE , due to bubble rearrangements. In the literature, these energy drops are often referred to as avalanches. Since the term “avalanche” tends to imply the existence of self-organized criticality, we employ the more neutral but less elegant term “energy drop.” The time interval between energy drops is much larger than the duration of a single event. This is also illustrated in Fig. 1(b), which shows the magnitude of energy drops that occur as the system is strained. (ΔE is scaled by the average energy per bubble E_b , which has been computed by averaging the elastic energy over the entire duration of a run and dividing by the total number of bubbles in the system, N_{bub} .) These recurring precipitous rearrangements represent the only way for the foam to relax stress: there is no mechanism involving a gradual energy release, as illustrated in Fig. 1(a). Note that we compute only the total elastic energy of the system; because events can be localized and intermittent, the elastic energy may be dropping in one region of the sample and rising in other regions. This would limit the size of the energy drop measured.

While useful for building intuition, the distribution of energy drops does not yield direct information about bubble rearrangements. Therefore, we also measure the number N of bubbles that experience a change in overlapping neighbors

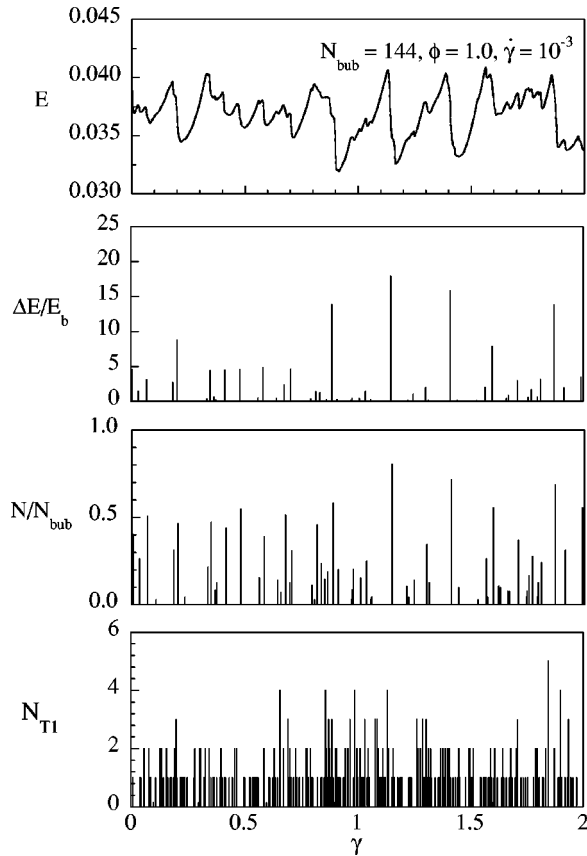


FIG. 1. Elastic energy and rearrangements vs strain for a 144-bubble system, with gas (area) fraction $\phi=1$, being slowly sheared at rate $\dot{\gamma}=10^{-3}$. The top plot (a) shows the total elastic energy stored in the “springs” of overlapping bubbles. Plot (b) shows the size of the energy drops that occur as the system is sheared. Note that the duration of an energy drop is very short compared to the time between energy drops at this low shear rate. Plot (c) shows the corresponding fraction of bubbles that experience a change in overlapping neighbors during each precipitous energy-drop event. The bottom plot (d) marks the mid-point of each $T1$ event, where two bubbles begin to intrude between two others; these have no direct correspondence to the energy drop events seen in (a) and (b). The behavior of all the properties shown here indicates that flow is accomplished inhomogeneously and intermittently by sudden rearrangements.

during an energy drop. In calculating distributions we exclude events in which two bubbles simply move apart or together; thus the smallest event is $N=3$. A typical sequence of configurations before, during, and after an event is shown in the first three frames of Fig. 2. In this energy drop the magnitude of the drop and the number of bubbles that change neighbors are close to the average. In the second and third frame of the sequence, we have marked the bubbles that changed neighbors since the beginning of the energy drop (shown in the first frame). As the system is strained, more bubbles change neighbors. For the particular energy drop chosen, roughly one-sixth of the bubbles eventually change overlapping neighbors. The fourth frame shows the final configuration of bubbles (colored gray) superimposed on the initial configuration at the start of the energy drop (colored black). Most of the bubble motions that lead to this average-sized energy drop are rather subtle shifts; there are no topo-

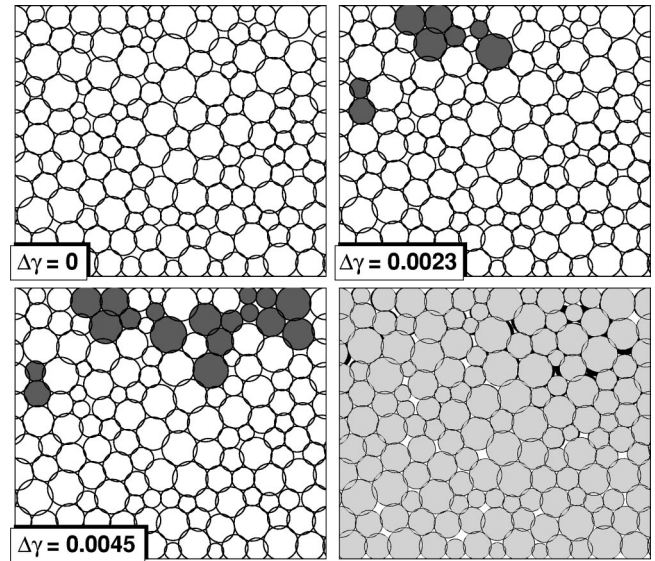


FIG. 2. Sequence of snapshots showing the nature of bubble rearrangements during an energy drop of average size in a 144-bubble system at $\phi=1.0$ sheared at a rate of $\dot{\gamma}=10^{-3}$. The magnitude of the drop ($\Delta E/E_b=2.61$) and the fraction of bubbles that change overlapping neighbors ($N/N_{bub}=0.18$) are both close to average. The first three frames show the configurations of bubbles at the start, middle and end of the energy drop, respectively. As the event proceeds, more and more bubbles change overlapping neighbors, as shown by the gray bubbles. The fourth frame shows the final configuration with bubbles in light gray superimposed on the initial configuration with bubbles in black. Most of the bubble motions involve subtle shifts of bubble positions; there are no topological rearrangements in this event. Note that although this event appears to nucleate at the top, in general the events appear randomly throughout the sample.

logical rearrangements. A large energy drop, from the tail of the distribution, is shown in Fig. 3. Again, the first three frames show the configurations at the beginning, middle and end of the drop, with the bubbles that change overlapping neighbors marked in gray. The fourth frame shows the extensive rearrangements that occur from the beginning to the end of the drop. The configuration shown is the final one, and the short segments are the tracks made by the centers of the bubbles during the energy drop.

Typically, larger drops involve larger numbers of bubbles. Figure 1(c) depicts N during each energy drop in the same run as in Figs. 1(a) and 1(b). (Here, N is normalized by the total number of bubbles in the system, N_{bub} .) The correlation between energy drops and the number of bubbles involved is shown by a scatter plot of these quantities in Fig. 4 for a 900-bubble system strained from 0 to 10. We see that indeed there is a strong correlation between these two measures of the size of an event. Larger drops in energy involve larger numbers of bubbles and are therefore spatially more extended. The correlation is particularly good at the large-event end. There is more variability for midsize and small events — a large range of energy drops corresponds to the same small number of rearranging bubbles, suggesting that typical rearrangements involve only a few bubbles.

Besides counting statistics for energy drops and changes in number of bubble overlaps, another direct measure of bubble rearrangements is the number of $T1$ events, i.e., of

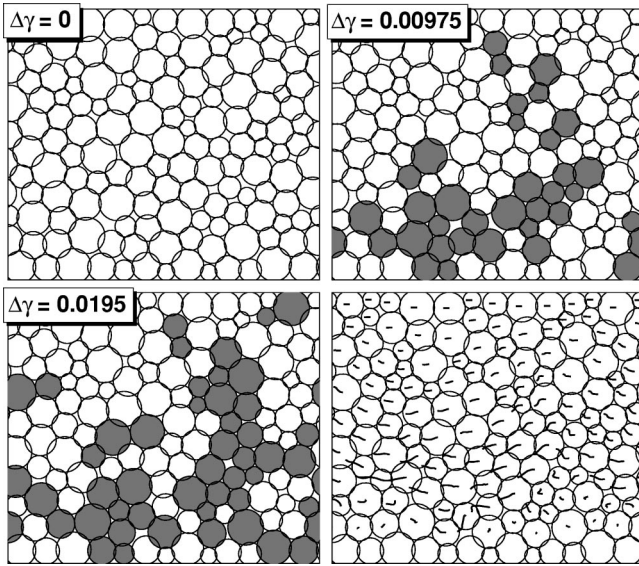


FIG. 3. Sequence of snapshots showing bubble rearrangements during a large energy drop in a 144-bubble system at $\phi=1.0$ and $\dot{\gamma}=10^{-3}$. The magnitude of the drop ($\Delta E/E_b=13.18$) and the fraction of bubbles that change overlapping neighbors ($N/N_{bub}=0.44$) both fall in the upper tails of the distributions. The first three frames show the configurations at the beginning, middle and end of the energy drop; the gray bubbles have changed overlapping neighbors since the start of the drop. The fourth frame shows the final configuration along with the tracks made by the centers of the bubbles during the event. We did not use the same scheme as in the fourth frame of Fig. 2 to show the rearrangements because the bubble motions were too extensive in this case.

topology changes of the first kind [3]. For a perfectly dry two-dimensional foam consisting of thin films, these are said to occur when a bubble edge shrinks to zero, such that a common vertex is shared by four bubbles, two moving apart and two moving together. These events were the only property used by Dennin and Knobler [7] to characterize the response of their monolayer foam to shear because they were unable to measure changes in the energy. While the time at which a $T1$ event occurs is well defined in a dry foam, it is somewhat ambiguous for a wet foam because there can be an exchange of nearest neighbors without a common point of contact. Moreover, while the number of bubbles involved in a $T1$ event is four by definition, large clusters of bubbles can

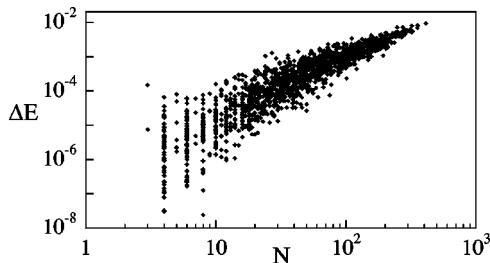


FIG. 4. The size of energy drops as a function of the number of bubbles that concurrently change overlapping neighbors during the energy drop, for a 900-bubble system at $\phi=1.0$ driven at $\dot{\gamma}=10^{-3}$. This indicates that the fraction of bubbles that change overlapping neighbors during an energy drop increases with the size of the energy drop.

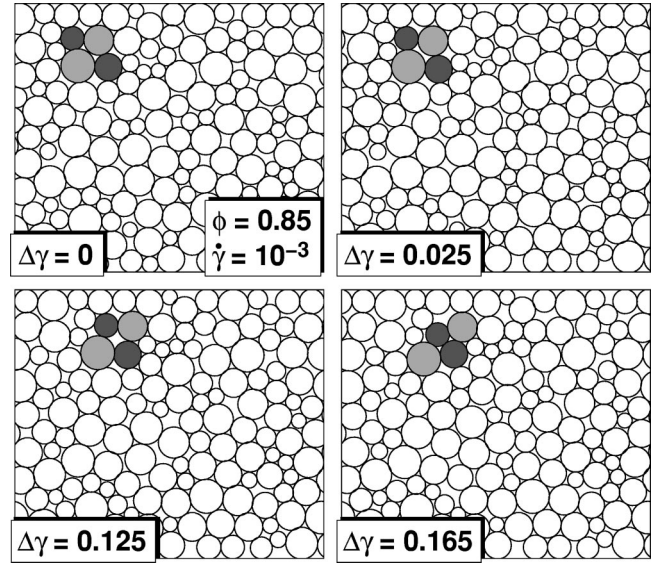


FIG. 5. A sequence of snapshots showing a $T1$ event in a wet foam at $\phi=0.85$ as the system is strained at $\dot{\gamma}=10^{-3}$. During the event, the black pair of bubbles moves together and the gray pair moves apart.

rearrange, with some of the interior bubbles being involved in two or three $T1$ events simultaneously. It is then much harder to assign an exact time to a $T1$ event.

To make contact with the monolayer experiments, we may define $T1$ events within the bubble model as follows. First we broaden the definition of “nearest neighbors” to also include bubbles that do not necessarily overlap, but that are nonetheless so close such that $|\vec{r}_i - \vec{r}_j| < a(R_i + R_j)$, where $a > 1$ is a suitably chosen factor that may depend on ϕ . We then say that a $T1$ event begins when two nearest neighbors move apart, and we say that it ends when a new nearest neighbor pair intrudes between them; the time at which the event occurs is taken as the midpoint in this sequence. This definition is illustrated in the time sequence of a $T1$ event shown in Fig. 5. While the duration of an actual $T1$ event in a dry foam is instantaneous, the duration within the bubble model may vary greatly. Furthermore, the midpoint in the sequence does not necessarily coincide with the exact moment the switching occurs. In many instances it takes a long time after two bubbles separate for the remaining pair to come into contact. To compare with our other measures of rearrangement, we depict in Fig. 1(d) the number of $T1$ events as a function of strain for the same run as in Figs. 1(a)–1(c). There appears to be some correlation between the largest energy drops and instances in which many $T1$ events occur simultaneously. However, there are many more $T1$ events than energy drops. This is because many $T1$ events can occur when a large cluster of bubbles rearranges, and because our definition also includes topology changes that cause an *increase* in the total elastic energy.

We can examine the consequences of our definition of a $T1$ event by studying the distribution of the number of rearrangement events as a function of their total duration in units of the strain. This is done for both energy drops and $T1$ events, as shown in Figs. 6(a) and 6(b). The duration of an energy drop is taken as the difference in strain between a decrease in the elastic energy and the next increase. It is

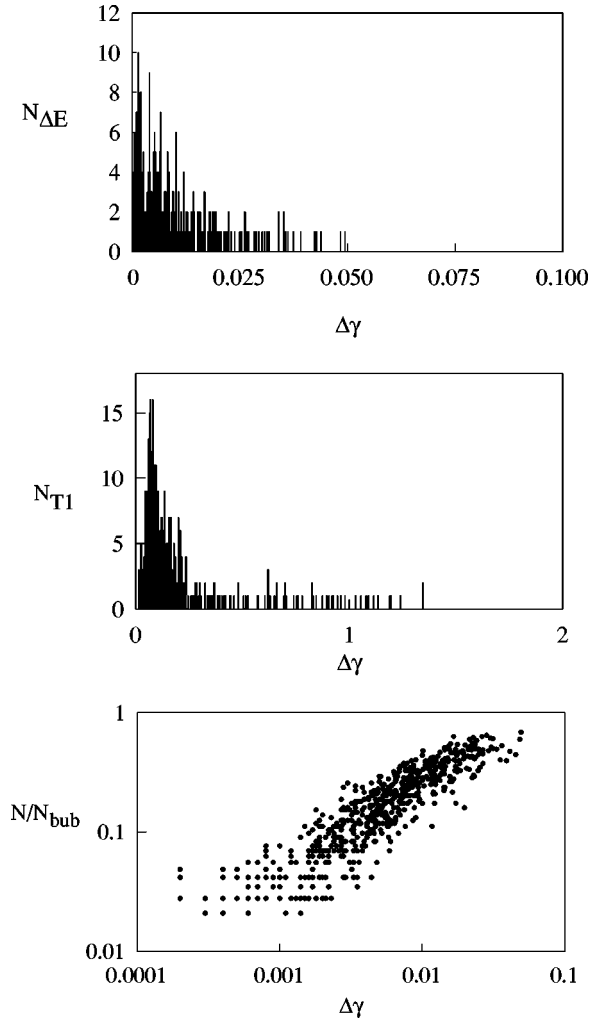


FIG. 6. The probability distribution for the duration of (a) energy-drop rearrangement events and (b) $T1$ events, for a 144-bubble system at $\phi=1$ driven at $\dot{\gamma}=10^{-3}$. Note that the typical duration of $T1$ events is significantly longer than that of energy drops. (c) Correlation plot of the fraction of bubbles involved in an energy drop vs the duration of the energy drop.

evident from the duration distribution for energy drops, Fig. 6(a), that most energy drops occur over a relatively short strain scale. In units of time, the longest events are comparable to a hundred times the characteristic time scale in the problem ($\tau_d=1$ in our simulations). As shown in Fig. 6(c), there is a good correlation between the number of bubbles that change overlapping neighbors and the duration of the event; the more bubbles involved in the event, the longer it lasts. The distribution for $T1$ events, shown in Fig. 6(b), has a qualitatively similar shape to the distribution of energy-drop events, but exhibits a slightly more rapid decrease for both fast and slow events. However, the scale on which $T1$ events occur is an order of magnitude larger than the characteristic duration of the energy drops. By examining the bubble motions we see that the largest energy drops are associated with many $T1$ events, but the difference in strain scales makes it difficult to demonstrate an exact correlation between the number of overlap changes and the number of $T1$'s. In counting the $T1$ events, we include only events that

have a total strain duration of less than 2. Figure 6(b) shows that we have included all the $T1$ events for this run.

V. SIMULATION RESULTS

For a given system size, strain rate, dissipation mechanism and gas fraction, we now collect statistics on the following measures of bubble dynamics: (1) The probability distribution $P(\Delta E)$ for energy drops of size ΔE ; (2) the probability distribution $P(N)$ for the number of bubbles N that change overlapping neighbors during an energy-drop event; and (3) the scaled event count for both energy drops and $T1$ events, $S(T1)$ and $S(\Delta E)$, both defined as the number of events per bubble per unit strain. With the exception of the 900-bubble system, for which only two runs were carried out, we have performed at least three different runs with different initial conditions for the same sets of parameters. We find that the measured quantities are insensitive to the initial conditions.

A. System size

We first address the important issue of the finite size of the simulation sample. This is done for dry foams, $\phi=1.0$, driven at a slow strain rate, $\dot{\gamma}=10^{-3}$. The results for four system sizes, $N_{bub}=36, 144, 324,$ and 900 , are shown in Fig. 7. In these runs, the systems were strained up to $80, 80, 31,$ and 10 , respectively. The top plot shows the energy-drop distribution scaled by E_b , the average energy per bubble. It shows that energy drops vary greatly in size over the course of a single run. The general features of this distribution have been reported earlier [13]. There is a power-law region with an exponent of -0.7 that extends over several decades in $\Delta E/E_b$, followed by a sharp cutoff that occurs above a characteristic event size. Such a distribution has a well-defined average energy drop, which is near the cutoff between $2E_b$ and $3E_b$ for the systems shown here. The slight deviation from power-law behavior for small ΔE was absent in the earlier simulations [13], which did not exclude two-bubble events, and which had a different roundoff error. Also, as seen earlier [13], the two largest systems, with 324 and 900 bubbles, respectively, have nearly identical distributions. This has two important implications; namely, that the sharp cutoff of the power-law distribution is not a finite-size effect, and that the system does not exhibit self-organized criticality.

The presence of a characteristic energy-drop size can be corroborated by examining the number of bubbles that participate in rearrangements for the same set of runs, which is given in the middle plot, Fig. 7(b). This quantity has not been studied previously within the bubble model. We plot the probability distribution $P(N)$ of the number of bubbles N that change overlapping neighbors during a rearrangement. The distribution decreases monotonically with a sharp cutoff at the large-event end. This indicates that most of the rearrangements are local and involve only a few bubbles. Figure 7(b) shows that as the system size increases, the largest events represent a smaller fraction of the total number of bubbles. Indeed, the tail of the distribution extends to smaller and smaller values of N/N_{bub} with no signs of saturation as the system size N_{bub} increases, indicating diminishing finite size effects.

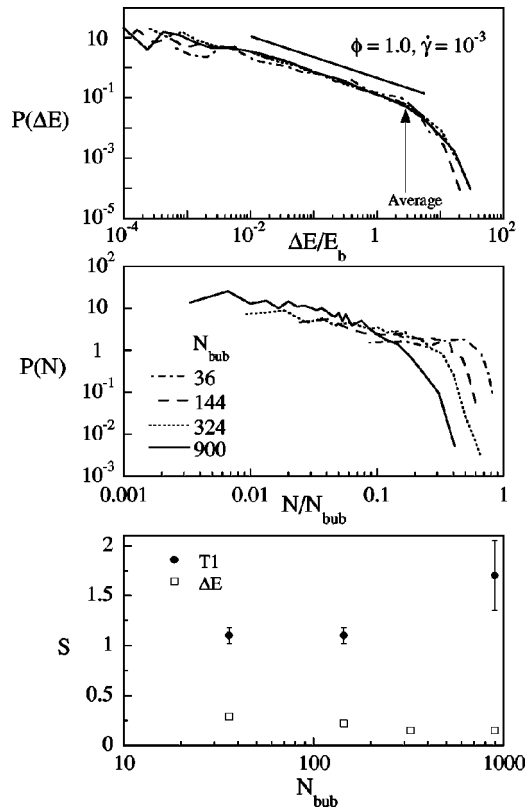


FIG. 7. Effect of system size at $\phi=1.0$ and $\dot{\gamma}=10^{-3}$. (a) Probability density distribution of energy drops ΔE scaled by E_b , the average energy per bubble for each run. There is a power-law region (the straight line has a slope of -0.7) followed by a sharp cutoff. The cutoff depends only weakly on the system size and converges for the larger systems. (b) Probability distribution of the number of bubbles that change overlapping neighbors during a rearrangement. The tails of the distribution extend to smaller fractions of the total number of bubbles in the system as the system size increases, showing that the events are spatially localized. (c) Event count for $T1$ events (solid circles) and energy drops (open squares). Error bars for $S(T1)$ in this and subsequent figures represent the variations found in independent runs (at least three, with the exception of the 900-bubble system for which only two runs were carried out) with the same parameters but different initial conditions. Where no error bar is indicated the variation is smaller than the size of the symbol. The number of energy drops per bubble decreases as the system size increases, reaching the same value for the 324-bubble and 900-bubble systems. There are, however, more $T1$ rearrangement events per bubble at the larger system size.

We next look at the system-size dependence of event counts, $S(T1)$ and $S(\Delta E)$, for the number of $T1$ events and energy drops per bubble per unit strain. This is shown in the bottom plot, Fig. 7(c), for the same runs as in Figs. 7(a) and 7(b). We find that $S(\Delta E)$ decreases very slightly with increasing system size, but saturates for the largest systems. The results for $S(T1)$ show a stronger system-size dependence, increasing slightly with N_{bub} . This could be due to the fact that bubbles on the top and bottom boundaries of the system are fixed, which lowers the number of possible $T1$ events per bubble. As the system size grows, the boundary bubbles represent a smaller fraction of the system so the event count increases towards its bulk value.

In short, all of our measurements at $\phi=1.0$ and $\dot{\gamma}=10^{-3}$ indicate that the rearrangement events are localized and that there is no self-organized criticality. This agrees with observations of rearrangements in both monolayer and bulk foams.

B. Shear rate dependence

Now that size effects have been ruled out for dry foams, we may examine the influence of shearing the sample at different rates. Experiments by Gopal and Durian [6] on three-dimensional foams show a marked change in the character of the flow with increasing shear rate. At low shear rates, the flow is characterized by intermittent, jerky rearrangement events occurring at a rate proportional to the strain rate. As the shear rate increases, so that the inverse shear rate becomes comparable to the duration of a rearrangement event, the flow becomes smoother and laminar, with all the bubbles gradually rearranging all the time. This was attributed to a dominance of viscous forces over surface tension forces when the strain rate exceeds the yield strain divided by the duration of a rearrangement event. In movies of our simulation runs, we also observe a crossover from intermittent, jerky rearrangements to smooth laminar flow. Similar smoothing has also been seen in stress vs. strain at increasing shear rates for the mean-field version of bubble dynamics [13]. This raises the question of how the statistics of rearrangement events change with shear rate. Specifically, how is the ‘‘smoothing out’’ of the flow reflected in the statistics at high rates, and is there a quasistatic limit at low shear strain rates, in which rearrangement behavior is independent of strain rate? Earlier numerical studies by Bolton and Weaire [10] were restricted, by construction, to the quasistatic limit. Okuzono and Kawasaki [8] examined nonzero shear rates, but focused only on establishing the low shear-rate limit. Recently, Jiang and co-workers found a strong dependence of the $T1$ event count on shear rate [14]. They found that the number of $T1$ events per bubble per strain, $S(T1)$, decreases sharply with strain rate with no evidence of a quasistatic limit.

Our results for rearrangement behavior vs strain rate are collected in Fig. 8 for a 144-bubble system at $\phi=1.0$. The top plot for the probability distribution of energy drops indicates that there is no gross change in $P(\Delta E)$ with shear rate, even though our movies show a smoothing with less frequent energy drops. However, there is some suppression of small energy drops with an accompanying increase at large energy drops, as reflected in a somewhat smaller power-law exponent and larger cutoff at high values of $\Delta E/E_b$. It is not apparent from $P(\Delta E)$ vs $\Delta E/E_b$, but we find that the average energy drop $\langle \Delta E \rangle$ and the average energy per bubble E_b both increase with shear rate, and that $\langle \Delta E \rangle$ increases more rapidly. The reason why E_b increases with shear rate is, of course, that viscous forces become more important than elastic forces and lead to increasing deformation (or in our model, overlaps) of bubbles. The net result is that there are fewer, relatively larger, rearrangements at high strain rates.

The tendency that small events are suppressed with increasing shear rates is also borne out by the distribution of the number of bubbles that change neighbors during an energy drop, as shown in Fig. 8(b). Note that unlike the previ-

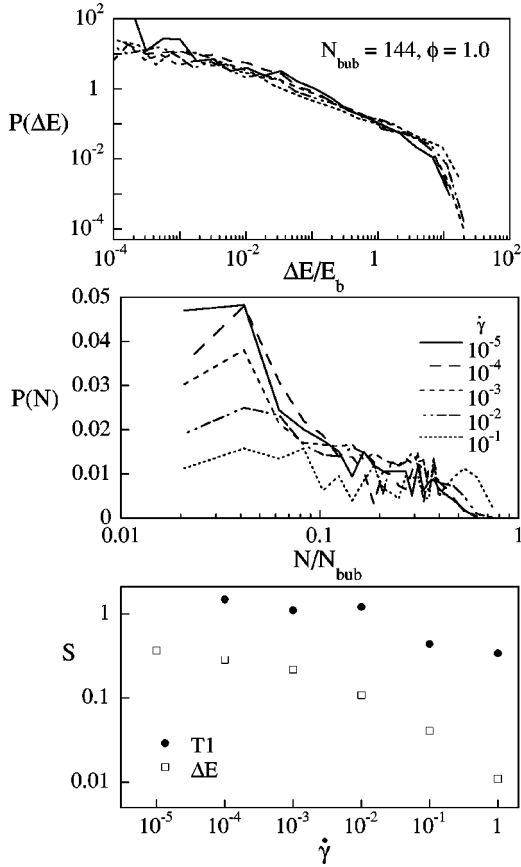


FIG. 8. Effect of shear rate for a 144-bubble system at $\phi = 1.0$. (a) There is no systematic change in the power-law region of the probability distribution of energy drops. The cutoff moves towards larger event sizes as $\dot{\gamma}$ increases. (b) A stronger trend is apparent in the probability distribution of rearranging bubbles. As $\dot{\gamma}$ increases, the distribution flattens. For the highest rate, $\dot{\gamma} = 0.1$, the distribution is fairly flat, suggesting that no one event size is dominant and the largest events are of the order of the system size. (c) Both the event counts for $T1$ events and energy drops decrease as the system is sheared faster. The $T1$ event counts at $\dot{\gamma} = 10^{-3}$ and 10^{-2} are the same within error. Note that a well-defined quasistatic limit is approached as $\dot{\gamma} \rightarrow 0$.

ous curves, $P(N)$ is plotted here on a linear scale. Two systematic trends emerge with increasing $\dot{\gamma}$: there are relatively fewer small events, i.e., $P(N)$ decreases significantly at small N/N_{bub} , and the tail extends to slightly higher N/N_{bub} . For $\dot{\gamma} = 10^{-1}$ the distribution is fairly flat, suggesting that no one event size is dominant and there are numerous large events of the order of the system size. This suggests that at this shear rate the system no longer relaxes stress by intermittent rearrangements, but by continuous flow, as confirmed by our movies of the runs [20]. The trend in $P(N)$ is seen in larger systems as well. For the 900-bubble system we also find that as the shear rate increases from 10^{-5} to 10^{-3} , the distribution flattens and extends to higher values of N . The average number of rearranging bonds increases with shear rate, consistent with the picture of many bubbles in motion as the system becomes more liquidlike. We cannot, however, probe the system at very high shear rates. Data above a shear rate of about 1 cannot be trusted because of the nature of the model used. At high rates of

strain the viscous term dominates and the elastic forces are not strong enough to prevent clumping of bubbles. This is actually an artifact of the assumption that only overlapping bubbles interact viscously; such clumping does not occur until much higher strain rates in the mean-field version of dynamics. Another reason why we do not study shear rates higher than unity is because we do not allow bubble breakup under flow (recall that $\dot{\gamma}$ is the capillary number).

The gradual smoothing with increasing shear rate is most apparent in Fig. 8(c), where we see that the event counts of $T1$ events and energy drops both decrease with increasing strain rate. For the $T1$ events, the decrease is slight, and is primarily due to the fact that the event duration becomes even longer. The decrease is more dramatic for the energy drop events. With increasing strain rate, the average energy drop increases and the rate of energy drops decreases.

Let us now reexamine the behavior of all quantities in Fig. 8, focusing on behavior at low shear strain rates. Note that all quantities appear to approach a reasonably well-defined ‘‘quasistatic’’ limit insensitive to the value of $\dot{\gamma}$. We thus have the following picture. For small $\dot{\gamma}$, the time between rearrangements is typically much longer than the duration of a rearrangement, implying there is adequate time for the system to relax stress. As the shear rate increases, bubbles are constantly in motion and cannot fully rearrange into local-minimum-energy configurations. Therefore, the viscous interactions dominate, and the system flows like an ordinary liquid.

C. Mean-field vs local dissipation

In the bubble model at higher strain rates, the behavior was seen to depend on the form of dissipation: clumping for local dissipation, Eq. (5), as opposed to no clumping for mean-field dissipation, Eq. (4). In this section we will investigate whether dissipation affects the low-strain-rate behavior as well. If there truly exists a quasistatic limit as $\dot{\gamma} \rightarrow 0$, as suggested by the plots in the previous section, then the form of dissipation should have no influence. This need not occur, since once a rearrangement starts it proceeds with finite speed according to dynamics set by a competition between surface tension and dissipation forces. For example, it is conceivable that the mean-field dynamics might discourage the mushrooming of a tiny shift in bubble position into a large avalanche, whereas local dynamics might not. Another important issue is that differences in mean-field vs local dissipation could be relevant to true physical differences between bulk foams and Langmuir monolayers at an air/water interface. For three-dimensional foams, the shear is transmitted through the sample via bubble-bubble interactions, so the dissipation might be better captured by the local dissipation model. In contrast, for two-dimensional Langmuir monolayer foams the subphase imposes shear on the monolayers, and the dissipation might therefore be closer to that calculated with the mean-field model.

To investigate the influence of mean-field vs local dynamics, we can simply compare avalanche statistics. This is done in Fig. 9 for 144-bubble systems at four different area frac-

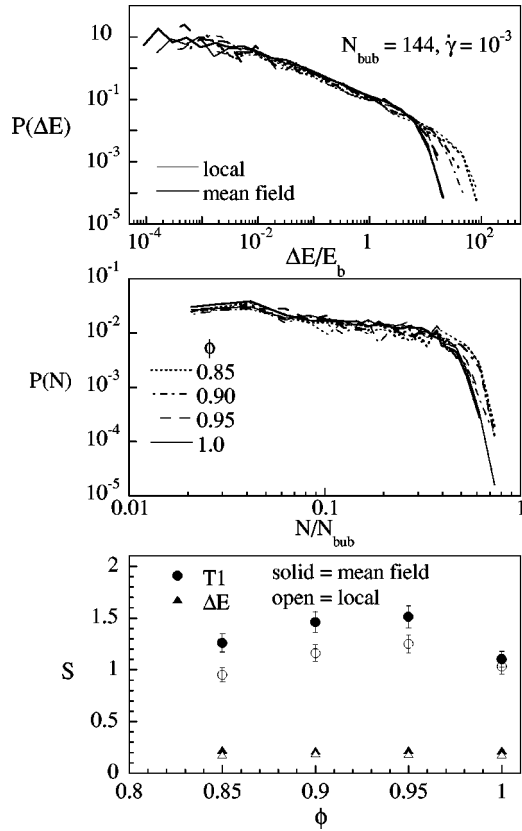


FIG. 9. Effect of gas area fraction and the form of viscous dissipation for a 144-bubble system sheared at $\dot{\gamma} = 10^{-3}$. The probability distribution of both (a) energy drops, and (b) number of bubbles changing overlapping neighbors during an event, are given at four area fractions: $\phi = 1.0, 0.95, 0.90$, and 0.85 . Heavy and light curves are for mean-field and local versions of dissipative dynamics, respectively. Note that the dynamics do not influence the behavior but that the events become larger as the gas fraction approaches the melting point, $\phi_c \approx 0.84$. Part (c) shows the event counts for $T1$ events and energy drops; these are insensitive to both gas area fraction and type of dynamics.

tions, all sheared at $\dot{\gamma} = 10^{-3}$. The top plot shows results for the energy-drop distribution, $P(\Delta E)$, with light (heavy) curves for local (mean-field) dissipation. There is no significant difference seen between the two choices of dissipative dynamics. This is also true of the spatial extent of the rearrangements, as seen in the middle plot for the probability distribution $P(N)$ of rearranging bubbles. The bottom plot for the rate of energy-drop and $T1$ events also shows little significant difference between mean-field and local dynamics. The only distinction is a slightly greater rate of $T1$ events in the mean-field case. This reflects the difference in duration of $T1$ events within the two models; we find that $T1$ events tend to last longer within the local dissipation model. Since we do not count $T1$ events that last longer than a strain of 2, we count fewer events within the local model than the mean-field version. Thus the differences in $S(T1)$ may simply be due to our method of counting $T1$ events. Taken together, the three plots in Fig. 9 encourage us to believe that the rearrangement dynamics predicted by the model are robust against details of the dissipation. They also provide further evidence for the existence of a true quasistatic limit,

where the effect of strain rate is *only* to set the rate of rearrangements.

D. Gas area fraction

Finally, we turn to the issue of how the elastic character of a foam disappears with increasing liquid content, and the possibility of critical behavior at the melting transition. The principal signature of the melting, or rigidity-loss, transition is that the shear modulus $G = \lim_{t \rightarrow \infty} \sigma(t)/\gamma$ vanishes and the foam can no longer support a nonzero shear stress without flowing. In two-dimensional systems, this happens at a critical gas fraction corresponding to that of randomly packed disks, $\phi_c \approx 0.84$. This has been seen in several different simulations, where the gas fraction was tuned to within 0.05 of the transition [9–11] and where it was tuned through, and even below, the transition [12,13]. Other signatures of melting are that the osmotic pressure vanishes as a power-law [12,13,16] the coordination number decreases towards about 4 as a power-law [9–13,21], and that the time scale for stress relaxation following an applied step-strain appears to diverge [12,13]. Here we look for signs of melting in the statistics of avalanches during slow, quasistatic flow. Within our model, an increase in liquid content causes a decrease in the average overlap between neighboring bubbles. This in turn produces a decrease in the average elastic energy of the system, E_b , and sets the scale for the average energy drop $\langle \Delta E \rangle$ per rearrangement. It therefore should also decrease at lower gas fractions ϕ .

The energy drop and size statistics of rearrangement events for increasingly wet foams were shown already in Fig. 9, but were discussed only in the context of mean-field vs local dissipative dynamics. A clear trend emerges when we examine the ϕ dependence specifically. In the top plot Fig. 9(a) for $P(\Delta E)$, we see that the power-law behavior for small events does not change, but that the exponential cut-off moves towards larger values of $\Delta E/E_b$ as $\phi \rightarrow \phi_c$. Though both $\langle \Delta E \rangle$ and E_b decrease towards zero, the latter evidently vanishes more rapidly. This results in a broader distribution of event sizes near the melting transition; as the system becomes more liquid, large events are more prevalent. The probability distribution $P(N)$ for the numbers of bubbles involved in rearrangement events is shown in Fig. 9(b). It displays similar trends as a function of ϕ , but not as pronounced as in $P(\Delta E)$. Namely, the power law for small N is unaffected by ϕ , but the exponential cutoff moves towards slightly larger events as $\phi \rightarrow \phi_c$. Thus, although the scale of energy drops increases dramatically, the number of broken bonds only increases marginally. Note, however, that the largest events include almost all the bubbles in the system; thus, the relatively weak dependence of $P(N)$ on ϕ could be a finite-size effect in these $N_{bub} = 144$ systems, as we will show below.

The behavior of S , the number of energy drops and $T1$ events per bubble per strain, is shown in Fig. 9(c). As the system becomes wetter, there is no noticeable change in the event number $S(\Delta E)$ for energy drops. In contrast, if our definition of nearest neighbors only includes overlapping bubbles, we find that $S(T1)$ decreases as ϕ decreases. This runs counter to expectations—bubbles in a wet foam should

have more freedom to move and rearrange because the energy barrier between rearrangements is lower and the yield strain is smaller. The apparent drop arises because the bubble coordination number is much higher in a dry foam (roughly 6) than in a wet foam (roughly 4). As a result there are more overlapping neighbors for each bubble in a dry foam, and more possibilities for the occurrence of $T1$ events. In the wet foam, however, there are many $T1$ events that do not satisfy the stringent starting or ending configurations because neighboring bubbles do not overlap. It is therefore appropriate in wet foams to modify the criterion for neighbors to $|\mathbf{r}_i - \mathbf{r}_j| < a(R_i + R_j)$, where the proximity coefficient a is taken as $1/\phi$. When $T1$'s are computed with this definition, we find no significant dependence on area fraction.

The fact that the power-law region of the energy-drop distribution is more extended at lower area fractions suggests the possibility of a critical point as the close-packing density, ϕ_c , is approached from above. This would imply a pure power-law distribution $P(\Delta E)$ for the energy drops at ϕ_c , which would presumably be accompanied by a growing correlation length, as well as the growing relaxation time observed previously in Refs. [12,13]. Note, however, that the distribution of the number of bubbles involved in a rearrangement, $P(N)$, does not depend very strongly on ϕ for the 144-bubble systems of Fig. 9; furthermore, the cut-off to power-law behavior is always present, no matter how closely ϕ_c is approached. This raises the question of whether finite system-size effects are more important at values of ϕ near ϕ_c (recall from Fig. 7 that there were no significant system-size effects near $\phi = 1$). To examine this, we have plotted the dependence of $P(\Delta E)$, $P(N)$ and S on system size in Fig. 10. We indeed find a strong system-size dependence in $P(\Delta E)$ at $\phi = 0.85$ just above the melting transition, with no saturation at the largest size studied (900 bubbles). This is consistent with the existence of a long correlation length.

The distribution of the number of bubbles per energy drop, $P(N)$ also shows signs of criticality. Recall from Fig. 7(b) that at $\phi = 1$, the tail of $P(N)$ was cut off at smaller and smaller values of N/N_{bub} with increasing system size at $\phi = 1$. This was consistent with a short correlation length, characteristic of localized rearrangement events. At $\phi = 0.85$, the behavior with increasing N_{bub} is quite different, as shown in Fig. 10(b). The distribution falls off slightly more rapidly with N/N_{bub} at larger system sizes (probably because $\phi = 0.85$ still lies above ϕ_c), but the largest events in the system still involve the same fraction $N/N_{bub} \approx 0.75$ of bubbles, indicating a correlation length that is comparable to the largest system size studied (30 bubble diameters across).

The event counts for energy drops and $T1$ events for the different system sizes at $\phi = 0.85$ are shown in Fig. 10(c). The behavior is not markedly different from that found for the drier foam. Recall, however, that we have adjusted our definition of a $T1$ event by changing the proximity coefficient a with area fraction, so little can be expected to be learned from this measure.

VI. DISCUSSION

We have reported the results of several different measures of rearrangement event dynamics in a sheared foam. A comparison of the probability distribution of energy drops

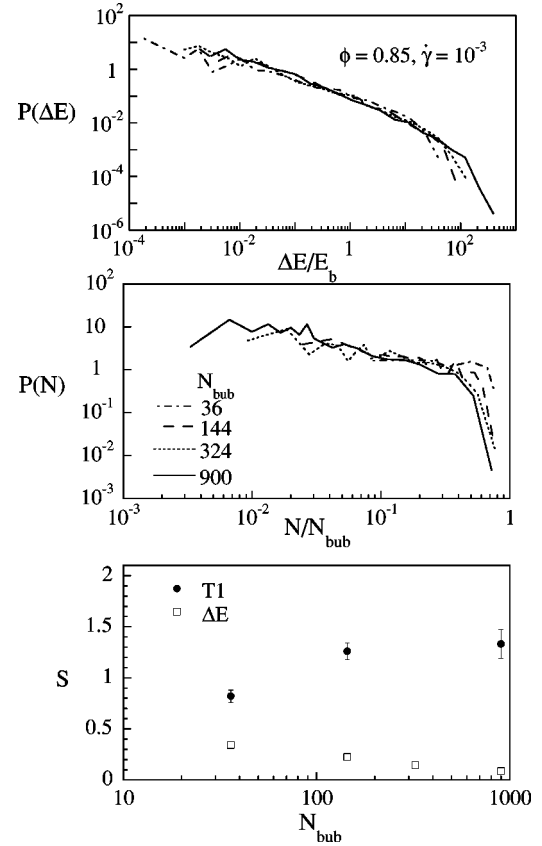


FIG. 10. Effect of system size at $\phi = 0.85$ and $\dot{\gamma} = 10^{-3}$. (a) There is no change in the power-law region of the probability density distribution compared with Fig. 6(a). However, the cutoff increases and there is no convergence for the largest system sizes. (b) Even at the largest system sizes, the largest events involve a significant fraction of the bubbles in the system, indicating that the events are much more spatially extended than at $\phi = 1$. (c) As in Fig. 7(c), the number of $T1$ events and energy drops show the opposite trend. The event count for energy drops indicate that finite size effects are more pronounced at this lower area fraction. Unlike the saturation seen in Fig. 7(c), the event number continues to drop as the system size increases.

$P(\Delta E)$ with the probability distribution of bubbles changing neighbors $P(N)$ shows that the size of an energy drop correlates well with the number of bubbles involved in a rearrangement (see Fig. 4). This is valuable because the energy drop-distribution has been widely studied theoretically, but is very difficult to measure experimentally. The number of bubbles involved in rearrangements, however, can be probed with multiple light scattering techniques on three-dimensional foams [5] and by direct visualization of two-dimensional foams [7]. A study of the rate of occurrence of topological changes ($T1$ events) provides a further link to experiments.

In general, our results agree with experiments on three-dimensional and two-dimensional foams. Despite its simplicity, the bubble model appears to capture the main qualitative features of a sheared foam remarkably well. For example, we find that the size of rearrangement events is typically small at low shear rates and at area fractions not too close to ϕ_c . This is in accord with experiments of Gopal and Durian [5], and Dennin and Knobler [7], as well as simulation results of

Bolton and Weaire [10] and Jiang and coworkers [14]. Our results do not agree with those of Okuzono and Kawasaki [8], however, who found power-law distributions of rearrangement events at $\phi=1$ in two dimensions.

The largest discrepancies between our results and those of others lie in the statistics of $T1$ events. We find that the number of $T1$ events per bubble per unit strain is of order unity and is generally insensitive to shear rate and gas area fraction. Kawasaki *et al.* [22] found similar results: $S(T1) = 0.5$ and no dependence on shear rate. In the Potts-model simulations [14], however, $S(T1)$ is unity at $\dot{\gamma} = 10^{-3}$ but falls to about 0.01 at $\dot{\gamma} = 10^{-1}$.

The monolayer experiments [7] yielded values of $S(T1) \approx 0.15$, nearly an order of magnitude lower than predicted by our simulations. Durian [13] reported a number of rearrangement events per bubble per unit strain for simulations of a 900-bubble system at $\dot{\gamma} = 10^{-5}$ that was comparable to the monolayer result, but he measured the number of energy drops per bubble per unit strain, $S(\Delta E)$, not the $T1$ event count, $S(T1)$. Note that our energy-drop event count, $S(\Delta E)$, agrees well with Durian's earlier result.

One might guess that the discrepancy between our measurement of $S(T1)$ and that of the monolayer experiment might lie in the method of analysis used to count $T1$ events. Unlike the simulations, in which the number of $T1$ events can be computed from an analysis of bubble positions as a function of time, the number of $T1$'s in the monolayer studies was determined by repeated viewing of videotapes of the experiments and counting of the events as the foam cells reach their midpoint configuration. It seemed possible, then, that the difference between the simulation and the experiment was the result of a systematic undercounting of the number of the events. To check this possibility, the number of $T1$'s in a simulation run was determined by observations of the animated bubble motions. The number of events missed in this unautomated counting was only 2% of the total.

We believe that the origin of the discrepancy between the $T1$ event rates in the simulation and the monolayer experiment lies in the yield strain. While the yield strain in the model system is less than 0.2, which is consistent with that measured in three-dimensional foams, that in the monolayer foams is closer to unity. Bubbles in monolayer foams can therefore sustain very large deformations without inducing rearrangements. The $T1$ event count should be inversely proportional to the yield strain. Thus, the ratio of $S(T1)$ in the simulation to $S(T1)$ in the experiment should equal the ratio of the yield strain in the experiment to the yield strain in the simulation. This is exactly what we find.

One of our main results is that a quasistatic limit exists within the bubble model. We find that the statistics of rearrangement events are independent of shear rate at low shear rates. This agrees with the monolayer experiments [7], which measured $T1$ event counts at two different shear rates, $\dot{\gamma} = 0.003 \text{ s}^{-1}$ and 0.11 s^{-1} . Dennin and Knobler found no noticeable difference in the $T1$ event count, despite the fact that the shear rates studied differ by a factor of thirty. In addition, Gopal and Durian found that the event rate, namely the number of rearrangement events per bubble per second, in a three-dimensional foam is given by the event rate in the

absence of shear plus a term proportional to the shear rate. In their case, the event rate was nonzero in the absence of shear because of coarsening; we have neglected this effect in our simulations. However, we do find that the rearrangement event rate (the product of S and the shear rate) is simply proportional to the shear rate at low shear rates. Thus, experimental results in both two and three dimensions contradict the simulation results of Jiang *et al.* [14], which find no quasistatic limit, but agree with our findings.

The form of dissipation used in the bubble model is a simple dynamic friction, which does not capture the hydrodynamics of fluid flow in the plateau borders and films in a realistic way. However, our results suggest that we may still be capturing the correct behavior at low shear rates. We find that the rearrangement event statistics are the same whether we use mean-field or local dissipation at low shear rates. This suggests that the statistics are determined by elastic effects rather than viscous ones at low shear rates, and that the behavior in that limit should be independent of the form of viscous dissipation used.

Finally, our results as a function of gas area fraction imply that there may be a critical point at the melting transition, as the area fraction approaches the random close-packing fraction from above. Previous studies showed that both the shear modulus and yield stress vanish as power laws at the melting transition [10,12], and that the stress relaxation time appears to diverge [12]. Here, we have shown by finite-size studies that there is also a correlation length, characterizing the size of rearrangements, which grows as one approaches the melting transition. We also find that the distribution of energy drops appears to approach a pure power law in that limit.

The existence of a critical point at the melting transition remains to be tested experimentally. The vanishing of the shear modulus and osmotic pressure at the transition has been measured by Mason and Weitz [23] for monodisperse, disordered emulsions, and by Saint-Jalmes and Durian for polydisperse gas-liquid foams [24]. However, these small-amplitude-strain rheological measurements could not test whether there is a diverging length scale for rearrangements in a steadily sheared system at the melting transition. On the other hand, Gopal and Durian [5] have measured the size of rearrangement events in a gas-liquid foam, but only at packing fractions well above the melting transition. At lower packing fractions close to the melting transition, the liquid drains too quickly from the foam due to gravity to permit such measurements. Experiments under microgravity conditions should be able to resolve whether the melting transition is indeed a critical point.

ACKNOWLEDGMENTS

We thank Narayanan Menon and Ian K. Ono for many helpful discussions, and we thank Michael Dennin for performing the visual analysis of the number of $T1$ events. This work was supported by the National Science Foundation through Grant Nos. CHE-9624090 (A.J.L.), CHE-9708472 (C.M.K.), and DMR-9623567 (D.J.D.), as well as by NASA through Grant No. NAG3-1419 (D.J.D.).

- [1] *Foams: Theory, Measurement, and Application*, edited by R. K. Prud'homme and S. A. Khan, Surfactant Science Series Vol. **57** (Marcel Dekker, New York, 1996).
- [2] D. J. Durian and D. A. Weitz, in *Kirk-Othmer Encyclopedia of Chemical Technology*, 4th ed., edited by J. I. Kroschwitz (Wiley, New York, 1994), Vol. 11, pp. 783–805.
- [3] D. Weaire and N. Rivier, *Contemp. Phys.* **25**, 55 (1984).
- [4] A.M. Kraynik, *Annu. Rev. Fluid Mech.* **20**, 325 (1988).
- [5] A.D. Gopal and D.J. Durian, *Phys. Rev. Lett.* **75**, 2610 (1995).
- [6] A. D. Gopal and D. J. Durian, *J. Coll. Interface Sci.* **213**, 169 (1999).
- [7] M. Dennin and C.M. Knobler, *Phys. Rev. Lett.* **78**, 2485 (1997).
- [8] T. Okuzono and K. Kawasaki, *Phys. Rev. E* **51**, 1246 (1995).
- [9] F. Bolton and D. Weaire, *Phys. Rev. Lett.* **65**, 3449 (1990).
- [10] F. Bolton and D. Weaire, *Philos. Mag. B* **65**, 473 (1992).
- [11] S. Hutzler, D. Weaire, and F. Bolton, *Philos. Mag. B* **71**, 277 (1995).
- [12] D.J. Durian, *Phys. Rev. Lett.* **75**, 4780 (1995).
- [13] D.J. Durian, *Phys. Rev. E* **55**, 1739 (1997).
- [14] Y. Jiang, P. J. Swart, A. Saxena, M. Asipauskas, and J. A. Glazier, *Phys. Rev. E* **59**, 5819 (1999).
- [15] X.F. Li, H. Zhou and C. Pozrikidis, *J. Fluid Mech.* **286**, 379 (1995).
- [16] The breakdown of pairwise additivity is discussed in M.D. Lacasse, G.S. Grest, D. Levine, T.G. Mason, and D.A. Weitz, *Phys. Rev. Lett.* **76**, 3448 (1996); M.D. Lacasse, G.S. Grest and D. Levine, *Phys. Rev. E* **54**, 5436 (1996).
- [17] DDRIV3 is available from <http://gams.nist.gov>. SPARSKIT2 was obtained from <ftp://ftp.cs.umn.edu>.
- [18] J.A. Glazier and D. Weaire, *J. Phys.: Condens. Matter* **4**, 1867 (1992).
- [19] J. Stavans, *Rep. Prog. Phys.* **56**, 733 (1993).
- [20] Quicktime movies of the bubble model simulation for fast and slow shear may be viewed at <http://math.nist.gov/mcsd/Staff/SLanger/foam>.
- [21] D. Weaire and S. Hutzler, *Physica A* **257**, 264 (1998).
- [22] K. Kawasaki, T. Okuzono, T. Kawakatsu, and T. Nagai in *Proceedings of the International Workshop of Physics of Pattern Formation*, edited by S. Kai (World Scientific, Singapore, 1992).
- [23] T.G. Mason, J. Bibette, and D.A. Weitz, *Phys. Rev. Lett.* **75**, 2051 (1995).
- [24] A. Saint-Jalmes and D. J. Durian (unpublished).